
Gated Cardiac $^{13}\text{N-NH}_3$ PET for Assessment of Left Ventricular Volumes, Mass, and Ejection Fraction: Comparison with Electrocardiography-Gated $^{18}\text{F-FDG}$ PET

Aliasghar Khorsand, PhD¹; Senta Graf, MD¹; Harald Eideherr, MD²; Wolfgang Wadsak, MD²; Kurt Kletter, MD²; Heinz Sochor, MD¹; Ernst Schuster, PhD³; and Gerold Porenta, MD, PhD⁴

¹Department of Cardiology, Medical University of Vienna, Vienna, Austria; ²Department of Nuclear Medicine, Medical University of Vienna, Vienna, Austria; ³Department of Medical Computer Sciences, Medical University of Vienna, Vienna, Austria; and ⁴Rudolfinerhaus, Vienna, Austria

The purpose of this study was to evaluate myocardial electrocardiography (ECG)-gated ^{13}N -ammonia ($^{13}\text{N-NH}_3$) PET for the assessment of cardiac end-diastolic volume (EDV), cardiac end-systolic volume (ESV), left ventricular (LV) myocardial mass (LVMM), and LV ejection fraction (LVEF) with gated $^{18}\text{F-FDG}$ PET as a reference method. **Methods:** ECG-gated $^{13}\text{N-NH}_3$ and $^{18}\text{F-FDG}$ scans were performed for 27 patients (23 men and 4 women; mean \pm SD age, 55 ± 15 y) for the evaluation of myocardial perfusion and viability. For both $^{13}\text{N-NH}_3$ and $^{18}\text{F-FDG}$ studies, a model-based image analysis tool was used to estimate endocardial and epicardial borders of the left ventricle on a set of short-axis images and to calculate values for EDV, ESV, LVEF, and LVMM. **Results:** The LV volumes determined by $^{13}\text{N-NH}_3$ and $^{18}\text{F-FDG}$ were 108 ± 60 mL and 106 ± 63 mL for ESV and 175 ± 71 mL and 169 ± 73 mL for EDV, respectively. The LVEFs determined by $^{13}\text{N-NH}_3$ and $^{18}\text{F-FDG}$ were $42\% \pm 13\%$ and $41\% \pm 13\%$, respectively. The LVMMs determined by $^{13}\text{N-NH}_3$ and $^{18}\text{F-FDG}$ were 179 ± 40 g and 183 ± 43 g, respectively. All *P* values were not significant, as determined by paired *t* tests. A significant correlation was observed between $^{13}\text{N-NH}_3$ imaging and $^{18}\text{F-FDG}$ imaging for the calculation of ESV ($r = 0.97$, SEE = 14.1, $P < 0.0001$), EDV ($r = 0.98$, SEE = 15.4, $P < 0.0001$), LVEF ($r = 0.9$, SEE = 5.6, $P < 0.0001$), and LVMM ($r = 0.93$, SEE = 15.5, $P < 0.0001$). **Conclusion:** Model-based analysis of ECG-gated $^{13}\text{N-NH}_3$ PET images is accurate in determining LV volumes, LVMM, and LVEF. Therefore, ECG-gated $^{13}\text{N-NH}_3$ can be used for the simultaneous assessment of myocardial perfusion, LV geometry, and contractile function.

Key Words: cardiac PET; ECG-gated acquisition; model-based image analysis; left ventricular function

J Nucl Med 2005; 46:2009–2013

Scientigraphic assessment of myocardial perfusion, metabolism, and cardiac function is commonly used in patients with proven or suspected cardiac disorders. Electrocardiography (ECG)-gated SPECT is routinely used for the determination of left ventricular (LV) function (1–3). PET with different tracers is a well-established method for the noninvasive assessment of myocardial perfusion and viability. Previously, gated $^{18}\text{F-FDG}$ PET was demonstrated to accurately determine LV volumes and contractile function (4–9). Cardiac ^{13}N -ammonia ($^{13}\text{N-NH}_3$) PET is frequently used to assess myocardial blood flow and coronary flow reserve (10–12). However, gated cardiac $^{13}\text{N-NH}_3$ imaging is currently not used for the estimation of LV function. The feasibility of a nearly simultaneous assessment of myocardial perfusion and contractile function through a combination of dynamic and ECG-gated acquisition protocols for $^{13}\text{N-NH}_3$ PET was reported earlier (13).

In a previous study, we used a model-based approach to gated cardiac $^{18}\text{F-FDG}$ imaging, in which the blurring effect in PET images is compensated for by computer-based modeling and estimates of systolic and diastolic cardiac volumes, LV ejection fraction (LVEF), and LV myocardial mass (LVMM) are derived. The accuracy of the results of gated $^{18}\text{F-FDG}$ studies was evaluated with measurements obtained from ECG-gated MRI as a reference method (8). Because the myocardial uptake of $^{13}\text{N-NH}_3$ and the myocardial uptake of $^{18}\text{F-FDG}$ are based on different principles (perfusion vs. metabolism) and because $^{13}\text{N-NH}_3$ images exhibit higher extracardiac activities, it remains undetermined whether a model-based image analysis also can be used for gated $^{13}\text{N-NH}_3$ PET images to derive accurate measurements of cardiac geometry and function.

Thus, it was the purpose of the present study to use model-based image analysis for ECG-gated $^{13}\text{N-NH}_3$ images to assess cardiac end-diastolic volume (EDV), cardiac

Received Jul. 15, 2005; revision accepted Sep. 14, 2005.

For correspondence or reprints contact: Aliasghar Khorsand, PhD, Department of Cardiology, Medical University of Vienna, Waehringer Guertel 18-20, A1090 Vienna, Austria.

E-mail: aliasghar.khorsand@meduniwien.ac.at

end-systolic volume (ESV), LVMM, and LVEF and to compare these results with measurements obtained from ECG-gated ^{18}F -FDG images.

MATERIALS AND METHODS

Patient Population

The patient population included 27 patients (23 men and 4 women; mean \pm SD age, 55 ± 15 y) who had coronary artery disease and who underwent gated ^{13}N - NH_3 and ^{18}F -FDG imaging as part of a 1-d study protocol for the evaluation of myocardial perfusion and viability between September 2001 and April 2005. One patient was excluded from the study because of poor quality of the gated ^{13}N - NH_3 images. All patients had a clinical history of myocardial infarction. As determined by visual analysis of PET images, 19 patients had an anterior myocardial infarction (8 small and 11 moderate or large) and 7 patients had an inferior myocardial infarction (3 small and 4 moderate or large). One patient presented with a normal tracer distribution on PET. Nine of the 27 patients (33%) showed a PET perfusion–metabolism mismatch.

PET Imaging

A high-spatial-resolution full-ring dedicated PET scanner (ADVANCE; GE Healthcare) was used to acquire gated images for both ^{13}N - NH_3 and ^{18}F -FDG during 8 cardiac phases covering the entire RR interval. After a 1-min scout scan for patient positioning, a 10-min transmission scan was obtained. For ^{13}N - NH_3 imaging, after an intravenous injection of 740 MBq of ^{13}N - NH_3 , a 5-min dynamic acquisition and then a 20-min gated acquisition were performed. For ^{18}F -FDG imaging, patients received a 75-g oral glucose load to enhance myocardial ^{18}F -FDG uptake and to increase the ratio of myocardial activity to background activity. Patients with diabetes were excluded from the glucose load. When the blood sugar level exceeded 140 mg/dL at 40 min after glucose loading, 2–8 IU of insulin were injected intravenously (2 IU for each 20 mg of glucose per deciliter over the level of 140 mg/dL). ^{18}F -FDG at 370 MBq was injected immediately thereafter. At 40 min after ^{18}F -FDG injection, ECG-gated image acquisition was performed for 20 min.

Transaxial gated ^{13}N - NH_3 and ^{18}F -FDG images were reconstructed with filtered backprojection by use of a Shepp Logan filter with a cutoff frequency of 0.48 cycle per centimeter, yielding an in-plane image resolution of 10 mm full width at half maximum. The reconstruction matrix was 128×128 pixels with a 2-mm pixel size. The short-axis views of both studies were created with GE Healthcare image processing software and were transferred to an image processing workstation (Onyx; Silicon Graphics) for further processing.

Image Analysis

Image analysis was performed with a semiautomated model-based method (8) that estimates endocardial and epicardial borders on a set of short-axis images and derives measurements of systolic and diastolic cardiac volumes. Processing tools and the graphical user interface for gated PET image analysis were developed with Interactive Data Language (IDL) software (CREASO).

The model-based method was based on a mathematic model of a radial activity profile obtained from cardiac short-axis images, incorporating the partial-volume effect, and therefore correcting the blurring effect on cardiac PET images. This model is fully specified by the blurring effect of the PET scanner (full width at

half maximum) and 5 parameters that are obtained from cardiac short-axis images: the LV radius, the LV wall thickness, and tracer activities in the blood pool, the myocardium, and the background (8).

For image processing, gated images that showed the smallest and largest LV cavities during a cardiac cycle were selected by visual inspection as end-systolic and end-diastolic frames. In both image sets, the most apical and basal slices were defined to indicate the range of images for further volume calculations. ^{13}N - NH_3 and ^{18}F -FDG image sets were analyzed by the same operator on separate days.

A circular region of interest was drawn with its center in the LV cavity of each selected short-axis slice, and 60 profiles then were generated along radial rays from the center of the left ventricle to the boundary of the circular region. Nonlinear regression analysis (14) was applied to fit the observed radial profile to the mathematic model and to obtain estimates for the LV radius and the LV wall thickness. Endocardial and epicardial contours were derived from the estimates of the LV radius and the LV wall thickness (Fig. 1). From these estimated borders, the endocardial and epicardial areas were calculated, and ESV and EDV were obtained by use of Simpson's rule. From the calculated volumes, global LVEF and LVMM were derived.

Statistical Analysis

Values are expressed as mean \pm SD. Group comparisons between ^{13}N - NH_3 and ^{18}F -FDG were performed by use of paired *t* tests. Regression analysis and Bland–Altman analysis (15) were used to elucidate the relationships between measurements from the 2 imaging methods. A *P* value of <0.05 was considered to indicate statistical significance.

RESULTS

Calculated LV volumes determined by ^{13}N - NH_3 and ^{18}F -FDG were 108 ± 60 mL and 106 ± 63 mL, respectively, at end systole and 175 ± 71 mL and 169 ± 73 mL, respec-

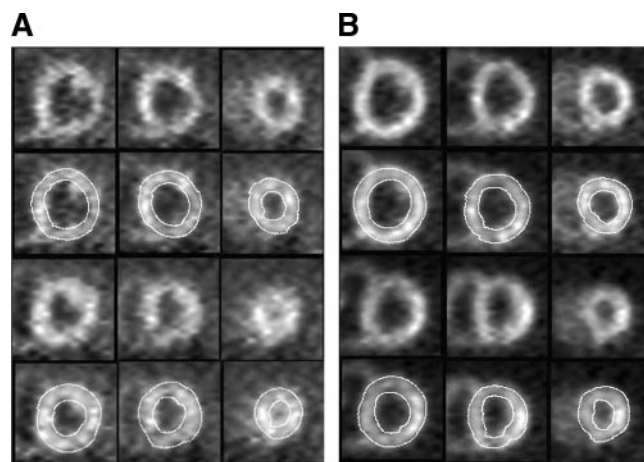


FIGURE 1. Example of model-based parameter estimation of cardiac geometry. Short-axis images obtained at basal, mid-ventricular, and apical levels (left to right) were derived from ^{13}N - NH_3 (A) and ^{18}F -FDG (B) PET studies for end-diastolic (upper 2 rows) and end-systolic (lower 2 rows) time points. Second and fourth rows depict short-axis views with overlays of estimated endocardial and epicardial contours.

TABLE 1
ESV, EDV, LVEF, and LVMM Determined from $^{13}\text{N-NH}_3$ and $^{18}\text{F-FDG}$ Images*

Method	Mean \pm SD for:			
	ESV (mL)	EDV (mL)	LVEF (%)	LVMM (g)
$^{13}\text{N-NH}_3$	108 \pm 60	175 \pm 71	42 \pm 13	179 \pm 40
$^{18}\text{F-FDG}$	106 \pm 63	169 \pm 73	41 \pm 13	183 \pm 43

*All *P* values were nonsignificant, as determined by paired *t* tests.

tively, at end diastole. The LVEFs determined by $^{13}\text{N-NH}_3$ and $^{18}\text{F-FDG}$ were 42% \pm 13% and 41% \pm 13%, respectively. The LVMMs determined by $^{13}\text{N-NH}_3$ and $^{18}\text{F-FDG}$ were 179 \pm 40 g and 183 \pm 43 g, respectively. The difference between measurements from the 2 imaging methods was not significant, as determined by paired *t* tests (Table 1).

A significant correlation was observed between $^{13}\text{N-NH}_3$ and $^{18}\text{F-FDG}$ studies for the calculation of ESV (ESV determined by $^{13}\text{N-NH}_3 = 0.92\text{ESV}$ determined by $^{18}\text{F-FDG} + 10.7$; $r = 0.97$, SEE = 14.1, $P < 0.0001$) (Fig. 2A), EDV (EDV determined by $^{13}\text{N-NH}_3 = 0.95\text{EDV}$ determined by $^{18}\text{F-FDG} + 13.2$; $r = 0.98$, SEE = 15.4, $P < 0.0001$) (Fig. 2C), LVEF (LVEF determined by $^{13}\text{N-NH}_3 = 0.9\text{LVEF}$ determined by $^{18}\text{F-FDG} + 4.8$; $r = 0.9$, SEE = 5.6,

$P < 0.0001$) (Fig. 3A), and LVMM (LVMM determined by $^{13}\text{N-NH}_3 = 0.87\text{LVMM}$ determined by $^{18}\text{F-FDG} + 19.4$; $r = 0.93$, SEE = 15.5, $P < 0.0001$) (Fig. 3C).

Bland–Altman analysis (Figs. 2B, 2D, 3B, and 3D) showed an excellent concordance between $^{13}\text{N-NH}_3$ and $^{18}\text{F-FDG}$ data; $^{13}\text{N-NH}_3$ yielded slightly higher values for volumes (2 \pm 15 mL for ESV and 6 \pm 16 mL for EDV) and LVEF (1% \pm 6%) but slightly lower values for LVMM (-4 ± 16 g).

Measurements of LVEF obtained for subgroups of patients with a small perfusion defect (47% \pm 12% by $^{13}\text{N-NH}_3$ vs. 46% \pm 13% by $^{18}\text{F-FDG}$) and with a moderate or large perfusion defect (38% \pm 15% by $^{13}\text{N-NH}_3$ vs. 38% \pm 11% by $^{18}\text{F-FDG}$) showed no significant difference between the 2 imaging methods. Moreover, when measurements of LVEF were compared for subgroups of patients with a perfusion–metabolism match (37% \pm 11% by $^{13}\text{N-NH}_3$ vs. 37% \pm 11% by $^{18}\text{F-FDG}$) or a perfusion–metabolism mismatch (52% \pm 11% by $^{13}\text{N-NH}_3$ vs. 50% \pm 9% by $^{18}\text{F-FDG}$), no significant difference between measurements obtained by $^{13}\text{N-NH}_3$ and those obtained by $^{18}\text{F-FDG}$ was found.

DISCUSSION

In this study, we compared ECG-gated $^{13}\text{N-NH}_3$ and $^{18}\text{F-FDG}$ PET for the assessment of LV volumes, LVEF, and LVMM in patients with coronary artery disease. The

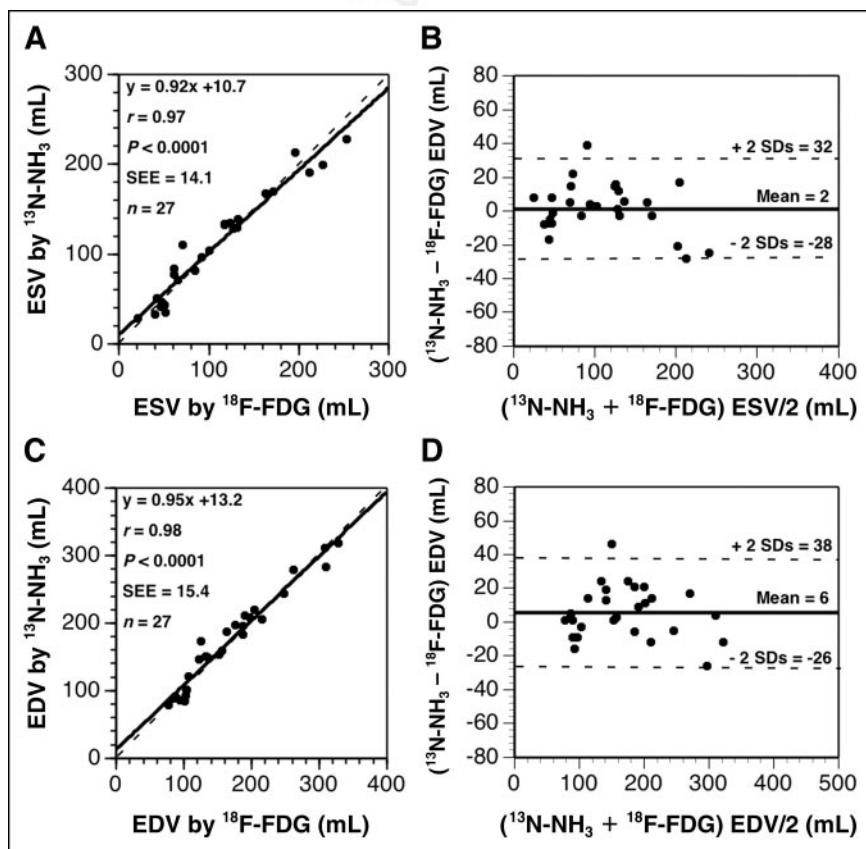


FIGURE 2. Regression analysis and Bland–Altman plots of ESV (A and B) and EDV (C and D) determined from $^{13}\text{N-NH}_3$ and $^{18}\text{F-FDG}$ PET images. Dashed lines in A and C are lines of identity ($^{13}\text{N-NH}_3$ value equals $^{18}\text{F-FDG}$ value). Mean differences and 95% confidence limits (± 2 SDs) in B and D are represented by solid and dashed lines, respectively.

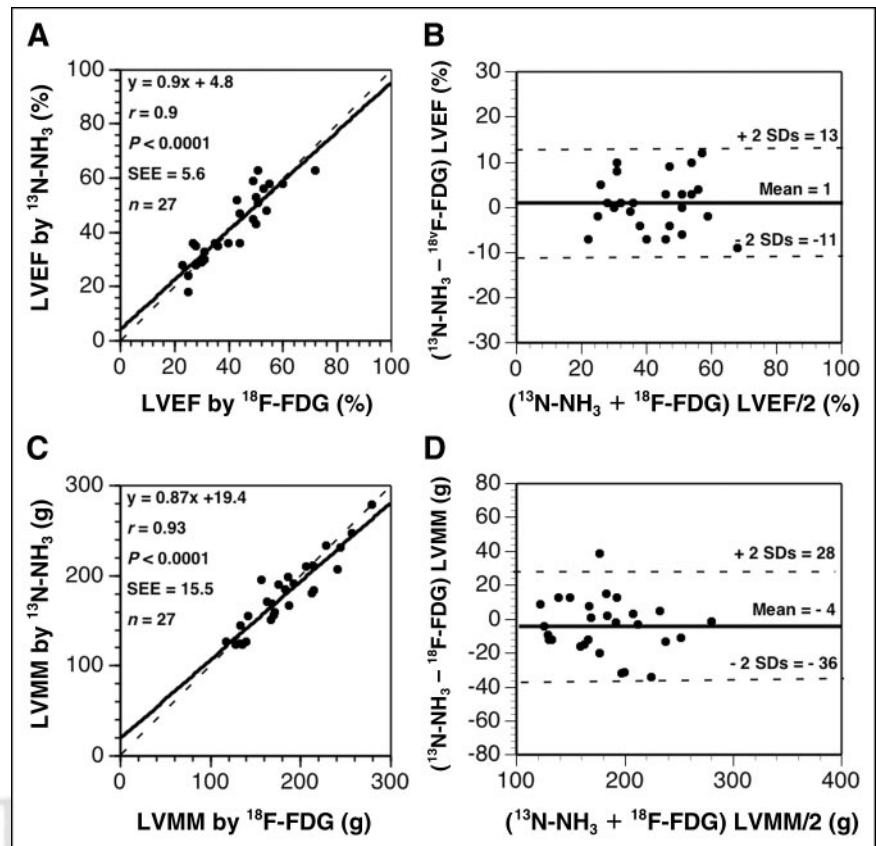


FIGURE 3. Regression analysis and Bland–Altman plots of LVEF (A and B) and LVMM (C and D) determined from $^{13}\text{N-NH}_3$ and $^{18}\text{F-FDG}$ PET images. Dashed lines in A and C are lines of identity ($^{13}\text{N-NH}_3$ value equals $^{18}\text{F-FDG}$ value). Mean differences and 95% confidence limits (± 2 SDs) in B and D are represented by solid and dashed lines, respectively.

results demonstrated excellent agreement between measurements from the 2 imaging methods. A direct comparison between $^{13}\text{N-NH}_3$ and $^{18}\text{F-FDG}$ by Bland–Altman analysis showed excellent concordance between the estimates of LV volumes, LVEF, and LVMM obtained by the 2 methods.

For both gated $^{13}\text{N-NH}_3$ and $^{18}\text{F-FDG}$ studies, we used a semiautomated model-based method that had been evaluated for gated $^{18}\text{F-FDG}$ in a previous study with measurements obtained from ECG-gated MRI as a reference method (8). That study showed that analysis of gated $^{18}\text{F-FDG}$ PET images with a model-based method yields measurements of LVEF, ESV, EDV, and LVMM similar to those derived from MRI. Other investigators evaluated ECG-gated $^{18}\text{F-FDG}$ PET with different image processing tools and radionuclide angiography (4,7), left ventriculography (5), or MRI (6,9) as a reference method and demonstrated that gated $^{18}\text{F-FDG}$ imaging is an accurate method for assessing LV volumes and contractile function.

In clinical practice, $^{13}\text{N-NH}_3$ is an established method for the quantitative imaging of myocardial blood flow at rest and under stress conditions and for measuring coronary flow reserve to evaluate the significance of coronary artery stenoses (16) as well as to detect microvascular disease (17). In addition, quantification of global LV function and its changes from rest to stress provides important prognostic information in coronary artery disease. In comparison, MRI is considered the reference method for the determination of

ventricular geometry and is used in clinical practice to assess myocardial viability by imaging of delayed contrast enhancement (18–20). However, in contrast to PET, MRI currently cannot provide reliable and accurate quantification of myocardial blood flow and cannot be used for patients with implanted devices, such as pacemakers or automatic defibrillators.

Simultaneous assessment of ventricular function and myocardial blood flow in the same imaging study is already in clinical use in myocardial perfusion SPECT and has been shown to offer important information beyond that provided by perfusion imaging alone. In fact, reduced LVEF increases the risk of cardiac death irrespective of the perfusion data, and the addition of ESV data further increases the diagnostic potential of gated SPECT (21). Although myocardial perfusion determined by SPECT is an established method that is performed frequently when ischemic cardiomyopathy is suspected, the inability of myocardial SPECT to quantify blood flow assigns PET a unique role in the assessment of ischemic cardiomyopathy. Thus, the capability of dynamic and ECG-gated $^{13}\text{N-NH}_3$ PET for the nearly simultaneous quantitative assessment of myocardial perfusion, coronary flow reserve, and contractile function should provide important information for patient management and risk stratification.

Okazawa et al. demonstrated the feasibility of assessing perfusion and function by using a single dose of $^{13}\text{N-NH}_3$ in

a group of healthy volunteers and in patients with cardiovascular disease (13). In that study, the calculated LVEF was compared with blood-pool imaging by $C^{15}O$ PET and left ventriculography; good agreement among these methods was found for patients with normal perfusion, whereas an underestimation of LVEF was found for patients with perfusion defects.

The reliability of estimation of endocardial and epicardial borders of the myocardium and calculation of LV volumes by model-based methods and by other methods based on myocardial tracer activity strongly depends on the quality of ECG-gated images. Acquisition of high-quality ECG-gated images requires a stable and regular cardiac rhythm throughout the entire acquisition period, a requirement that may not be fulfilled in patients with heartbeat irregularities, such as atrial fibrillation or multiple extrasystoles.

In studies with limited image quality or with segments with reduced tracer uptake, contour interpolation was used to estimate the LV radius and the LV wall thickness. This method leads to acceptable results for small defects and for larger regions with reduced tracer uptake. However, estimation of endocardial and epicardial borders in studies with large defects in tracer uptake leads to unreliable results (8). In particular, image quality is of major relevance for the estimation of wall thickness. Decreased regional count activity and segmental interpolation may result in incorrect estimates of regional wall thickness and LVMM. However, global parameters of LV function, such as calculation of LV volumes or LVEF, can be assessed accurately, as these parameters are less affected by low image quality or large defects in tracer uptake.

CONCLUSION

In conclusion, LV volumes, LVMM, and contractile function can be accurately measured from ECG-gated cardiac $^{13}N-NH_3$ images by use of a model-based analysis technique to determine endocardial and epicardial borders. Cardiac $^{13}N-NH_3$ PET with static, dynamic, and ECG-gated image acquisition thus offers a nearly simultaneous assessment of myocardial perfusion and contractile function.

ACKNOWLEDGMENTS

The authors thank the technologists of the PET Center of the Department of Nuclear Medicine for their technical assistance in performing the cardiac PET studies. This work was partly supported by a research grant provided by the Verein zur Förderung der Wissenschaftlichen Forschung am Rudolfinerhaus.

REFERENCES

1. Germano G, Kiat H, Kavanagh PB, et al. Automatic quantification of ejection fraction from gated myocardial perfusion SPECT. *J Nucl Med.* 1995;36:2138–2147.
2. Faber TL, Cooke CD, Folks RD, et al. Left ventricular function and perfusion from gated SPECT perfusion images: an integrated method. *J Nucl Med.* 1999; 40:650–659.
3. Faber TL, Vansant JP, Pettigrew RI, et al. Evaluation of left ventricular endocardial volumes and ejection fractions computed from gated perfusion SPECT with magnetic resonance imaging: comparison of two methods. *J Nucl Cardiol.* 2001;8:645–651.
4. Willemsen AT, Siebelink HJ, Blanksma PK, Paans AM. Automated ejection fraction determination from gated myocardial FDG-PET data. *J Nucl Cardiol.* 1999;6:577–582.
5. Hattori N, Bengel FM, Mehilli J, et al. Global and regional functional measurements with gated FDG PET in comparison with left ventriculography. *Eur J Nucl Med.* 2001;28:221–229.
6. Rajappan K, Livieratos L, Camici PG, Pennell DJ. Measurement of ventricular volumes and function: a comparison of gated PET and cardiovascular magnetic resonance. *J Nucl Med.* 2002;43:806–810.
7. Saab G, Dekemp RA, Ukkonen H, Ruddy TD, Germano G, Beanlands RS. Gated fluorine 18 fluorodeoxyglucose positron emission tomography: determination of global and regional left ventricular function and myocardial tissue characterization. *J Nucl Cardiol.* 2003;10:297–303.
8. Khorsand A, Graf S, Frank H, et al. Model-based analysis of electrocardiography-gated cardiac ^{18}F -FDG PET images to assess left ventricular geometry and contractile function. *J Nucl Med.* 2003;44:1741–1746.
9. Schaefer WM, Lipke CS, Nowak B, et al. Validation of QGS and 4D-MSPECT for quantification of left ventricular volumes and ejection fraction from gated ^{18}F -FDG PET: comparison with cardiac MRI. *J Nucl Med.* 2004;45:74–79.
10. Schelbert HR, Phelps ME, Huang SC, et al. N-13 ammonia as an indicator of myocardial blood flow. *Circulation.* 1981;63:1259–1272.
11. Kühle WG, Parenta G, Huang SC, et al. Quantification of regional myocardial blood flow using ^{13}N -ammonia and reoriented dynamic positron emission tomographic imaging. *Circulation.* 1992;86:1004–1017.
12. Hutchins GD, Schwaiger M, Rosenspire KC, Krivokapich J, Schelbert H, Kuhl DE. Noninvasive quantification of regional blood flow in the human heart using N-13 ammonia and dynamic positron emission tomographic imaging. *J Am Coll Cardiol.* 1990;15:1032–1042.
13. Okazawa H, Takahashi M, Hata T, Sugimoto K, Kishibe Y, Tsuji T. Quantitative evaluation of myocardial blood flow and ejection fraction with a single dose of ^{13}N -ammonia and gated PET. *J Nucl Med.* 2002;43:999–1005.
14. Marquardt D. An algorithm for least-squares estimation of non-linear parameters. *J Soc Ind Appl Math.* 1963;11:431–441.
15. Bland JM, Altman DG. Statistical methods for assessing agreement between two methods of clinical measurement. *Lancet.* 1986;1:307–310.
16. Muzik O, Duvernoy C, Beanlands RS, et al. Assessment of diagnostic performance of quantitative flow measurements in normal subjects and patients with angiographically documented coronary artery disease by means of nitrogen-13 ammonia and positron emission tomography. *J Am Coll Cardiol.* 1998;31:534–540.
17. Gould KL, Kirkeeide RL, Buchi M. Coronary flow reserve as a physiologic measure of stenosis severity. *J Am Coll Cardiol.* 1990;15:459–474.
18. Kim RJ, Wu E, Rafael A, et al. The use of contrast-enhanced magnetic resonance imaging to identify reversible myocardial dysfunction. *N Engl J Med.* 2000;343: 1445–1453.
19. Mahrholdt H, Wagner A, Holly TA, et al. Reproducibility of chronic infarct size measurement by contrast-enhanced magnetic resonance imaging. *Circulation.* 2002;106:2322–2327.
20. Gerber BL, Garot J, Bluemke DA, Wu KC, Lima JA. Accuracy of contrast-enhanced magnetic resonance imaging in predicting improvement of regional myocardial function in patients after acute myocardial infarction. *Circulation.* 2002;106:1083–1089.
21. Sharir T, Germano G, Kavanagh PB, et al. Incremental prognostic value of post-stress left ventricular ejection fraction and volume by gated myocardial perfusion single photon emission computed tomography. *Circulation.* 1999;100: 1035–1042.